Volume 60
Number 69
7 September 2024
Pages 9119–9286

ChemComm

Chemical Communications

rsc.li/chemcomm

ISSN 1359-7345

ROYAL SOCIETY OF CHEMISTRY

COMMUNICATION

Katarzyna N. Jarzembska *et al.*

Pressure-induced single-crystal-to-single-crystal nitrite ligand isomerisation accompanied by a piezochromic effect

60 YEARS ANNIVERSARY

ChemComm

COMMUNICATION

View Article Online
View Journal | View Issue

Check for updates

Cite this: *Chem. Commun.*, 2024, **60**, 9194

Received 14th June 2024,
Accepted 22nd July 2024

DOI: 10.1039/d4cc02898h

rsc.li/chemcomm

Open Access Article. Published on 24 July 2024. Downloaded on 6/16/2025 4:29:33 PM.
This article is licensed under a Creative Commons Attribution 3.0 Unported Licence.

Pressure-induced single-crystal-to-single-crystal nitrite ligand isomerisation accompanied by a piezochromic effect†

Kinga Potempa, [a] Damian Paliwoda, [b] Katarzyna N. Jarzembska, *[a] Radosław Kamiński, [a] Adam Krówczyński, [a] Patryk Borowski [a] and Michael Hanfland [c]

High-pressure structural study of a piezochromic crystal of a rare di-*exo*-nitrito nickel(II) complex supported by computational analysis is presented. The examined system is not photoswitchable, however, in the 0–6.2 GPa pressure range the crystal undergoes two phase-transitions accompanied by a colour change and the nitrite ligand isomerisation, which is unique.

Stimuli-responsive materials, which change their properties under the influence of external factors, have been attracting increasing attention over the years.[1–3] This is due to their potential wide applications as sensors, catalysts, optoelectronic switches, storage devices, *etc.*[4–6] Changes of materials' properties are often driven by changes in their structure at the molecular level. Thus, crystals constitute convenient model systems to study such processes in the solid state using spectroscopic and crystallographic methods.[7–15]

High pressure (HP) is among the factors which affect materials' structure. By applying HP one can stimulate some transformations and/or control properties of a given material. To date various HP-induced solid-state reactions, such as single-crystal-to-single-crystal polymerization,[16,17] tautomerisation,[18] cycloaddition[19] and isomerisation[20–22] were reported. However, as far as the linkage isomerism is concerned, to the best of our knowledge, only studies on the HP C≡N-group isomerisation, which affected magnetic properties of the examined material, were successful.[23,24] Indeed, such reactions are most often triggered by light and/or temperature changes and can be accompanied by photochromic effects.[25–31] In the case of nitro-to-nitrito isomerisation, there are no literature reports on its initiation by HP. For instance, in work by Zakharov *et al.*[32] only unit-cell parameter changes and phase transitions were noted, while no NO_2-group isomerisation was detected. This observation goes along with our yet unpublished results on a couple of square-planar nitro nickel complexes,[33] which showed that the nitro isomer cannot be transformed into the nitrito form upon HP, while this transformation is well activated optically at temperatures below 240 K. In all these cases, in the ground-state crystal structure the nitro-(η^1-N(O)$_2$) linkage isomer was either the only form, or the dominant one, which could have been transformed into an *endo*- and/or *exo*-nitrito-(η^1-O–N=O) isomer. Among the mentioned linkage isomers, the *exo*-nitrito binding mode is, in general, the least observed one.[8,26,33–36] However, introducing a compound which would primarily exist in the form of the rare *exo*-nitrito binding mode, which has a significantly different shape than the other two, would open the possibility of the *exo*-nitrito-to-nitro/*endo*-nitrito solid-state transformation *e.g.* induced by compression. In such a case, the *exo*-nitrito isomer, which is itself often less stable than the other nitrite forms, needs to be well-supported by the crystal environment. As far as the limited examples of iron(II),[37] cobalt(III),[38] manganese(III)[39] or nickel(II)[40–43] nitrite coordination compounds are concerned, it seems that the octahedral geometry and large and flat aromatic ancillary ligand may favour formation of the *exo*-nitrito binding mode in the ground-state crystal structure.

In view of the above, a simple nickel(II) nitrite coordination compound (hereafter **Ni-diONO**, Fig. 1a), reported around 50 years ago by Campbell and Urbach, was selected based on its molecular structure (yet no X-ray diffraction – XRD – data was reported).[44] This octahedral complex molecule possesses two nitrite groups above and below the plane of a flat, rather rigid and symmetric tetradentate *N*,*N*′-bis(2-pyridylmethylene)-1,3-diaminopropanone ligand that coordinates to the triplet nickel centre *via* four nitrogen atoms. The compound has significant switching potential, while its specific geometry may lead to the desired crystal packing, supporting a non-standard binding mode of the nitrite groups.

[a] *Department of Chemistry, University of Warsaw, Żwirki i Wigury 101, 02-089 Warsaw, Poland. E-mail: katarzyna.jarzembska@uw.edu.pl*
[b] *European Spallation Source ERIC, Partikelgatan 2, 224 84 Lund, Sweden*
[c] *European Synchrotron Radiation Facility, 71 avenue des Martyrs, 38043 Grenoble, France*

† Electronic supplementary information (ESI) available: synthesis, sample characterization, (HP)XRD measurements, structure analyses, NMR. CCDC 2352765–2352783. For ESI and crystallographic data in CIF or other electronic format see DOI: https://doi.org/10.1039/d4cc02898h

This journal is © The Royal Society of Chemistry 2024

Open Access Article. Published on 24 July 2024. Downloaded on 6/16/2025 4:29:33 PM.
This article is licensed under a Creative Commons Attribution 3.0 Unported Licence.

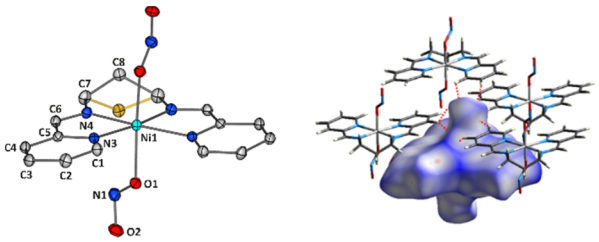

Fig. 1 (a) Molecular structure of **Ni-diONO** derived from the 100 K XRD data. Note both NO_2 groups exhibit the *exo*-nitrito binding mode. Atomic thermal motion is represented as ellipsoids (50% probability level; symmetry-induced disorder at the C8 atom is shown in yellow). (b) Hirshfeld surface generated for **Ni-diONO** mapped with the d_{norm} property.[45]

Based on the 100 K single-crystal X-ray diffraction data the compound crystallizes in the *C*2/*c* space group with half a molecule in the asymmetric unit (ASU; Table 1). Some disorder is observed only for the C8 carbon atom, which forms a molecular tip that can equally well be directed upwards or downwards relative to the plane of the tetradentate ligand. Since the (*N*,*N*′,*N*,*N*′)-donor ligand contains two aromatic fragments, it imposes a certain way of molecular packing in the crystal structure so as to optimise the π···π stacking interactions (Fig. S5.1, ESI†) and possibly satisfy also the secondary intermolecular contacts (Fig. 1b). Each **Ni-diONO** molecule forms effective π···π stacking interactions with four neighbouring species, rotated by the 2-fold symmetry axis. Consequently, some relatively narrow cavities are left to host the nitrite groups above and below the ancillary ligand. As a result, **Ni-diONO** exists exclusively in the targeted di-*exo*-nitrito form.

Indeed, similarly to other compounds of this kind, as far as the isolated molecule of **Ni-diONO** is concerned, the *exo*-nitrito isomer is not energetically favoured (Table S4.1, ESI†).[8,28,33,34] However, this compound does not entirely follow the energetic patterns of other nitrite nickel complexes. Based on the density functional theory computations, the energetic differences between the examined isomers are not very pronounced, whereas the nitro isomer, which is usually considered to be the most energetically stable one as an isolated molecule, is slightly less advantageous than the *endo*-nitrito binding mode - the most preferred nitrite form of **Ni-diONO**. Taking into account subtle differences in molecular energies, volume and shape of the available space (Fig. S5.2, ESI†) and intermolecular interactions, the *exo*-nitrito isomer is definitely the one best supported by the crystal structure. This is confirmed by the computational analysis of the interaction energy of dimeric motifs formed by the considered linkage isomers (Table S5.5, S5.3 and S5.4, ESI†).

The *exo*-nitrito group is involved in five noteworthy intermolecular contacts with the adjacent ancillary ligands as denoted in Fig. 1b. These are two hydrogen bonds formed by each of the nitrite oxygen atoms with the heterocyclic aromatic rings on the sides, and the C–H···N interaction. Furthermore, the protruding O2 oxygen atom interacts with the aromatic fragment located above *via* two C–H···O-type contacts. During heating of the system from 100 K to room temperature (r.t.), its space-group symmetry lowers from *C*2/*c* to *Cc*. This is due to residual dynamic disorder which shows up at the nitrite ligands at higher temperature and eliminates the 2-fold symmetry (Fig. S2.2, ESI†). It appears, the unit cell expands (by 2.8%) mainly along the *a* (1.4%) and *c* (∼1%) edges, while the hydrogen bonds engaging the nitrite moiety become more distant and weaker (Fig. S5.3, ESI†). In consequence, the reaction cavity volume increases, enabling rotation around the N–O bond, which manifests in the *ca.* 6–8% disorder on each *exo*-nitrito ligand.

As expected, there is no light effect on the binding mode of the nitrite group in the studied system. For nickel nitrite complexes this stimulus usually triggers the opposite nitro-to-nitrito isomerisation. In this regard, it was worth verifying the impact of HP on the di-*exo*-nitrito **Ni-diONO** crystal structure.

HP XRD synchrotron studies were conducted in a stepwise pressure-increase manner up to 6.15(5) GPa, and then the sample was gradually decompressed back to ambient conditions. During this process two phase transitions occurred, accompanied by the nitrite ligand isomerisation and crystal-colour change from yellow to orange to red (Fig. 2). The observed transformations appeared to be entirely reversible (Fig. S6.1, ESI†). Phase **I** is sustained up to 2.15(5) GPa with the *Cc* space-group symmetry. In the 0–2.15 GPa pressure range, compression causes typical decrease of the unit cell volume (by 11%). The most significant contraction occurs along the *a* (6.4%) dimension (*b*↓ by 2.8%, *c*↓ by 3.4%). Hydrogen bonds engaged in stabilization of the *exo*-nitrito moieties get shortened and less beneficial due to the pressure-induced tensions (Tables S5.7 and 5.8, ESI†). This is especially visible for such interaction between aromatic rings and the protruding *exo*-nitrito oxygen atom, which starts to press on the aromatic fragment upon compression. Similarly, the C8–H8b···O2 contact undergoes significant shortening, which also has the destabilizing effect, leading to a notable disorder of the nitrite ligand at the N1 site at 2.15(5) GPa. Crystal voids get reduced by *ca.* 58 Å^3, thus, only 26 Å^3 of free space is left in the unit cell. The main bits of the free space remain right in-between the adjacent nitrite ligands (Fig. S6.2, ESI†).

Table 1 Selected **Ni-diONO** crystal-structure parameters derived from the 100 K and r.t. XRD data at various pressures (see also Table S2.1, ESI)

Ni-diONO	Phase $\mathbf{I_{LT}}$ (see ESI)	Phase **I**	Phase **II**	Phase **III**
Formula	$C_{15}H_{16}N_6NiO_4$			
Crystal colour	Yellow	Yellow	Bright orange	Dark orange
T [K]	100	r.t.	r.t.	r.t.
P [GPa]	Ambient	Ambient	2.88(2)	3.98(2)
Crystal system	Monoclinic	Monoclinic	Triclinic	Triclinic
Space group	*C*2/*c*	*Cc*	$P\bar{1}$	$P\bar{1}$
Z/*Z*′	$4/\frac{1}{2}$	4/1	6/3	4/2
a [Å]	13.559(3)	13.750(3)	19.686(4)	12.396(2)
b [Å]	9.666(2)	9.663(2)	9.307(2)	9.204(2)
c [Å]	13.263(3)	13.387(3)	12.765(3)	12.618(3)
α [°]	90	90	90.02(3)	90.26(3)
β [°]	111.25(3)	110.53(3)	106.67(3)	105.54(3)
γ [°]	90	90	105.24(3)	87.17(3)
V [Å^3]	1620.1(7)	1665.7(7)	2154.4(9)	1385.3(5)
V/*Z* [Å^3]	405.0(2)	416.4(2)	359.1(2)	346.3(1)

Open Access Article. Published on 24 July 2024. Downloaded on 6/16/2025 4:29:33 PM.
This article is licensed under a Creative Commons Attribution 3.0 Unported Licence.

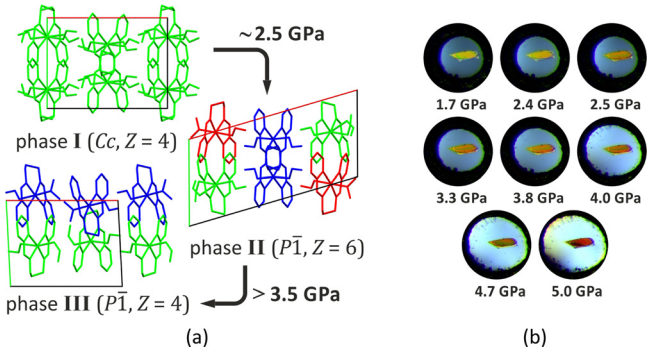

Fig. 2 (a) Crystal packing of different phases (view along Z axis, colours distinguish symmetry-inequivalent molecules). (b) Crystal colour recorded at various pressures.

Around 2.5 GPa the first phase transition occurs and the symmetry of the crystal structure lowers from Cc to $P\bar{1}$ (Fig. 2a). Phase **II** is rather temporal, as it exists only in the narrow pressure range from about 2.5 to about 3.5 GPa. The unit-cell changes significantly along the a dimension, which gets extended *ca.* 1.5 times, while the γ angle becomes more obtuse, reaching *ca.* 105°. In consequence, 6 molecules fill such a skewed and elongated unit cell instead of 4. Furthermore, each of the 3 symmetry-independent molecules constitutes a different isomer (Fig. S2.2, ESI†). The first molecule adopts the di-*exo*-nitrito binding mode, whereas in the two remaining moieties the nitrite group opposite to the C8 molecular tip of the ancillary ligand undergoes isomerisation. It either transforms fully to the nitro form, or adopts the disordered *endo*-nitrito binding mode (Fig. 3 and Fig. S2.2, ESI†).

As a consequence of the applied pressure, molecules rearrange in the crystal structure so the amount of the free space compared to the unit-cell volume decreases (Fig. 3; V_{void}/V ratio *vs.* applied pressure, where V_{void} – total volume of the crystal voids, V – unit-cell volume; Table S6.1, ESI†). In the first stage the decline is significant, then the curve begins to flatten,

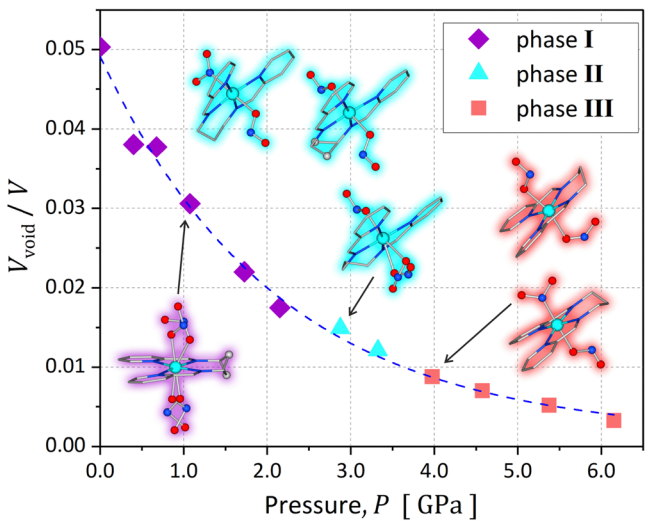

Fig. 3 V_{void}/V ratio *vs.* applied pressure; ASU content depicted.

which is especially visible once the first phase transition occurs. The trend can be well described by an exponential decay function, in contrast to parabolic decrease of V/Z (Fig. S6.1, ESI†). In the case of phase **III** the $P\bar{1}$ space group is preserved, however, the a parameter of the unit cell almost returns back to that of phase **I**. The unit cell hosts 4 molecules, whereas both symmetry-independent species exhibit one fully transformed nitrite moiety, on the side opposite to the molecular C8 tip of the ancillary ligand (Fig. 3 and Fig. S2.2, ESI†). In one molecule it is the *endo*-nitrito binding mode, while in the other – the nitro conformation. The isomerised nitrite sites face one another in the crystal structure.

Analysis of the intermolecular interactions (Fig. S5.5, and Table S5.8, ESI†) indicates that if the ambidentate ligands remain in the *exo*-nitrito configuration, in general the same set of interactions is preserved throughout the examined pressure range. In turn, as far as the nitro and *endo*-nitrito binding modes are concerned, although the general interaction pattern with three adjacent ancillary ligands is maintained, the intermolecular contacts get notably distorted. This is manifested in a significant change in the space occupied by these ligands as shown in Fig. S6.3 (ESI†). In the case of the nitro and *endo*-nitrito fragments, facing one another, the reaction cavity is spread between the molecular layers parallel to the (100) crystal plane. Based on that and changes of distances between nickel centres, it is clear that mechanically induced linkage isomerism constitutes a way to reduce stress in the crystal structure of **Ni-diONO**. Indeed, the Ni···Ni distance on the side of the isomerised nitrite groups at 6.15(5) GPa is almost 1 Å shorter than that on the side of the *exo*-nitrito. In the crystal structure of phase **III**, which is itself very compact (Fig. S6.2, ESI†), main fragments of free space are still found in the vicinity of nitrite ligands. The total achieved unit-cell volume compression reached 20.8%, with the most significant shortening of the a unit-cell dimension (~12%).

Overall, by carefully selecting of a nitrite nickel(II) complex of a specific molecular structure, it was possible to impose formation of the rare *exo*-nitrito binding mode in the crystal structure, which is unique. In consequence, the photoswitchable properties of the resulting material were hampered, but a possibility of a mechanically-stimulated nitrite ligand isomerisation opened up. The applied pressure affects most the unit-cell dimension parallel to the *exo*-nitrito moiety resulting in its isomerisation, as both *endo*-nitrito and nitro binding modes require less space in this direction.[33] This is the first observation of the pressure-induced nitrite group isomerisation. Structural changes, including two phase transitions, are accompanied by the crystal-colour change. Such behaviour is typical for crystal structures stabilised by π-stacking interactions.[20–22] Indeed, here the aromatic fragments come closer one to another and form less symmetric interactions as the pressure increases (Fig. S6.4 and S6.5, ESI†). Nevertheless, according to the calculated UV-Vis spectra (Fig. S8.1, ESI†) linkage isomerism may also contribute to the observed piezochromism. The results indicate new interesting application perspectives of nitrite-based molecular switches.

 This journal is © The Royal Society of Chemistry 2024

K. P. and K. N. J acknowledge the Polish National Science Centre for financial support (2020/38/E/ST4/00400, SONATA BIS; 2019/35/O/ST4/04197, PRELUDIUM BIS grants). The access to ESRF was funded by the Polish Ministry of Science and Higher Education (2021/WK/11, CH-6469). XRD experiments were co-financed by EU (POIG.02.01.00-14-122/09). WCSS (grant No. 285) is acknowledged for providing computational facilities.

Data availability

The data supporting this article have been included as part of the ESI.†

Conflicts of interest

There are no conflicts to declare.

References

1 P. Naumov, S. Chizhik, M. K. Panda, N. K. Nath and E. Boldyreva, *Chem. Rev.*, 2015, **115**, 12440–12490.
2 A. Chaudhary, A. Mohammad and S. M. Mobin, *Cryst. Growth Des.*, 2017, **17**, 2893–2910.
3 S. Saha, M. K. Mishra, C. M. Reddy and G. R. Desiraju, *Acc. Chem. Res.*, 2018, **51**, 2957–2967.
4 W. M. Awad, D. W. Davies, D. Kitagawa, J. Mahmoud Halabi, M. B. Al-Handawi, I. Tahir, F. Tong, G. Campillo-Alvarado, A. G. Shtukenberg, T. Alkhidir, Y. Hagiwara, M. Almehairbi, L. Lan, S. Hasebe, D. P. Karothu, S. Mohamed, H. Koshima, S. Kobatake, Y. Diao, R. Chandrasekar, H. Zhang, C. C. Sun, C. Bardeen, R. O. Al-Kaysi, B. Kahr and P. Naumov, *Chem. Soc. Rev.*, 2023, **52**, 3098–3169.
5 D. Yan, Z. Wang and Z. Zhang, *Acc. Chem. Res.*, 2022, **55**, 1047–1058.
6 Y. Ye, H. Hao and C. Xie, *CrystEngComm*, 2022, **24**, 3136–3149.
7 E. Ahmed, S. Chizhik, A. Sidelnikov, E. Boldyreva and P. Naumov, *Inorg. Chem.*, 2022, **61**, 3573–3585.
8 A. Mikhailov, K. A. Konieczny, M. Gladysheva, P. Plyusnin, S. Pillet and D. Schaniel, *Inorg. Chem.*, 2023, **62**, 5531–5542.
9 L. E. Hatcher, J. M. Skelton, M. R. Warren, C. Stubbs, E. L. D. Silvaa and P. R. Raithby, *Phys. Chem. Chem. Phys.*, 2018, **20**, 5874–5886.
10 T. Friščić, L. R. MacGillivray and Z. Kristallogr, *Cryst. Mater.*, 2005, **220**, 351–363.
11 S.-L. Huang, T. S. A. Hor and G.-X. Jin, *Coord. Chem. Rev.*, 2017, **346**, 112–122.
12 J. W. Lauher, F. W. Fowler and N. S. Goroff, *Acc. Chem. Res.*, 2008, **41**, 1215–1229.
13 Q.-Q. Li, C.-Y. Ren, Y.-Y. Huang, J.-L. Li, P. Liu, B. Liu, Y. Liu and Y.-Y. Wang, *Chem. – Eur. J.*, 2015, **21**, 4703–4711.
14 D. Kitagawa, K. Kawasaki, R. Tanaka and S. Kobatake, *Chem. Mater.*, 2017, **29**, 7524–7532.
15 T. Galica, J. Bąkowicz, K. Konieczny and I. Turowska-Tyrk, *Cryst. Growth Des.*, 2018, **18**, 1636–1644.
16 H. Zheng, K. Li, G. D. Cody, C. A. Tulk, X. Dong, G. Gao, J. J. Molaison, Z. Liu, M. Feygenson, W. Yang, I. N. Ivanov, L. Basile, J.-C. Idrobo, M. Guthrie and H.-K. Mao, *Angew. Chem., Int. Ed.*, 2016, **55**, 12040–12044.
17 T. Poręba, M. Ernst, D. Zimmer, P. Macchi and N. Casati, *Angew. Chem., Int. Ed.*, 2019, **58**, 6625–6629.
18 Y. Wang, X. Tan, Y.-M. Zhang, S. Zhu, I. Zhang, B. Yu, K. Wang, B. Yang, M. Li, B. Zou and S. X.-A. Zhang, *J. Am. Chem. Soc.*, 2015, **137**, 931–939.
19 B.-B. Ni, K. Wang, Q. Yan, H. Chen, Y. Ma and B. Zou, *Chem. Commun.*, 2013, **49**, 10130–10132.
20 X. Meng, G. Qi, C. Zhang, K. Wang, B. Zou and Y. Ma, *Chem. Commun.*, 2015, **51**, 9320–9323.
21 X. Deng, H. Guo, X. Meng, K. Wang, B. Zou and Y. Ma, *Chem. Commun.*, 2019, **55**, 4663–4666.
22 X. Meng, C. Chen, G. Qi, X. Li, K. Wang, B. Zou and Y. Ma, *ChemNanoMat*, 2017, **3**, 569–574.
23 E. Coronado, M. C. Giménez-López, T. Korzeniak, G. Levchenko, F. M. Romero, A. Segura, V. García-Baonza, J. C. Cezar, F. M. F. Groot, A. Milner and M. Paz-Pasternak, *J. Am. Chem. Soc.*, 2008, **130**, 15519–15532.
24 E. Coronado, M. C. Giménez-López, G. Levchenko, F. M. Romero, V. García-Baonza, A. Milner and M. Paz-Pasternak, *J. Am. Chem. Soc.*, 2005, **127**, 4580–4581.
25 M. R. Warren, S. K. Brayshaw, A. L. Johnson, S. Schiffers, P. R. Raithby, T. L. Easun, M. W. George, J. E. Warren and S. J. Teat, *Angew. Chem., Int. Ed.*, 2009, **48**, 5711–5714.
26 L. E. Hatcher, J. Christensen, M. L. Hamilton, J. Trincao, D. R. Allan, M. R. Warren, I. P. Clarke, M. Towrie, S. Fuertes, C. C. Wilson, C. H. Woodall and P. R. Raithby, *Chem. – Eur. J.*, 2014, **20**, 3128–3134.
27 K. A. Deresz, R. Kamiński, S. E. Kutniewska, A. Krówczyński, D. Schaniel and K. N. Jarzembska, *Chem. Commun.*, 2022, **58**, 13439–13442.
28 P. Borowski, K. N. Jarzembska, R. Kamiński, K. Durka and D. Schaniel, *Cryst. Growth Des.*, 2023, **23**, 5986–5997.
29 N. Casaretto, S. Pillet, E. E. Bendeif, D. Schaniel, A. K. E. Gallien, P. Klufers and T. Woike, *IUCrJ*, 2015, **2**, 35–44.
30 B. Cormary, S. Ladeira, K. Jacob, P. G. Lacroix, T. Woike, D. Schaniel and I. Malfant, *Inorg. Chem.*, 2012, **51**, 7492–7501.
31 I. R. Laskar, D. Das, G. Mostafa, T.-H. Lu, T.-C. Keng, J.-C. Wang, A. Ghosh and N. R. Chaudhuri, *New J. Chem.*, 2001, **25**, 764–768.
32 B. A. Zakharov, A. S. Marchuk and E. V. Boldyreva, *CrystEngComm*, 2015, **17**, 8812–8816.
33 K. Potempa, K. A. Deresz, J. Jankowska, K. N. Jarzembska, A. Krówczyński, A. Mikhailov, D. Schaniel and R. Kamiński, *Chem. – Eur. J.*, 2023, **29**, e202302629.
34 S. E. Kutniewska, A. Krówczyński, R. Kamiński, K. N. Jarzembska, S. Pillet, E. Wenger and D. Schaniel, *IUCrJ*, 2020, **7**, 1188–1198.
35 S. E. Kutniewska, R. Kamiński, W. Buchowicz and K. N. Jarzembska, *Inorg. Chem.*, 2019, **58**, 16712–16721.
36 M. R. Warren, T. L. Easun, S. K. Brayshaw, R. J. Deeth, M. W. George, A. L. Johnson, S. Schiffers, S. J. Teat, A. J. Warren, J. E. Warren, C. C. Wilson, C. H. Woodall and P. R. Raithby, *Chem. – Eur. J.*, 2014, **20**, 5468–5477.
37 D. M. M. M. Dissanayake, B. E. Petel, W. W. Brennessel, K. L. Bren and E. M. Matson, *J. Coord. Chem.*, 2020, **73**, 2664–2676.
38 M. S. Møller, J. Kongsted and C. J. McKenzie, *Dalton Trans.*, 2021, **50**, 4819–4829.
39 M. Strianese, S. Milione, V. Bertolasi and C. Pellecchia, *Inorg. Chem.*, 2013, **52**, 11778–11786.
40 S. Ghosh, H. Deka, S. Saha and B. Mondal, *Inorg. Chim. Acta*, 2017, **466**, 285–290.
41 M. G. B. Drew and S. Hollis, *Acta Cryst. Sect. B*, 1980, **36**, 1944–1947.
42 N. F. Curtis and M. P. Coles, *Polyhedron*, 2017, **127**, 369–389.
43 R. Cortes, M. I. Arriortua, T. Rojo, X. Solans and D. Beltran, *Polyhedron*, 1986, **5**, 1987–1990.
44 T. G. Campbell and F. L. Urbach, *Inorg. Chem.*, 1973, **12**, 1836–1840.
45 M. A. Spackman and D. Jayatilaka, *CrystEngComm*, 2009, **11**, 19–32.

Open Access Article. Published on 24 July 2024. Downloaded on 6/16/2025 4:29:33 PM. This article is licensed under a Creative Commons Attribution 3.0 Unported Licence.